Applied Catalysis A: General 392 (2011) 45–56

Contents lists available at ScienceDirect

Applied Catalysis A: General

journal homepage: www.elsevier.com/locate/apcata

# Combustion of diesel soot in $NO/O_2$ presence. Cesium nitrate and gold catalysts

María L. Ruiz[a], Ileana D. Lick[b], Marta I. Ponzi[a], Enrique Rodriguez-Castellón[c], Antonio Jiménez-López[c], Esther N. Ponzi[b,*]

[a] INTEQUI (CONICET-UNSL), 25 de Mayo N° 384, Villa Mercedes, San Luis, 5730, Argentina
[b] CINDECA (CCT-La Plata-CONICET-UNLP), Departamento de Química, Facultad de Ciencias Exactas, calle 47 N° 257, La Plata, Buenos Aires, 1900, Argentina
[c] Departamento de Química Inorgánica, Cristalografía y Mineralogía, Facultad de Ciencias, Universidad de Málaga, Campus de Teatinos, Málaga, 29071, Spain

ARTICLE INFO

*Article history:*
Received 4 August 2010
Received in revised form 15 October 2010
Accepted 20 October 2010
Available online 27 October 2010

*Key words:*
Diesel soot
Cesium nitrate
Gold
Combustion

ABSTRACT

The diesel soot combustion was studied using catalysts prepared by impregnation with cesium nitrate and/or gold on zirconium oxide ($ZrO_2$), hydrated zirconium oxide and silica ($SiO_2$). Catalysts were characterized by colorimetry, elemental analysis, atomic absorption spectrophotometry, XRD, FTIR, TPR and XPS. Measurements of catalytic activity were performed in a thermobalance with air and in a fixed bed reactor with a $NO/O_2$ feed. All catalysts containing cesium nitrate exhibit a good activity for soot oxidation and the addition of gold substantially increases the $CO_2$ generation leading the selectivity to 100% in $CO_2$.



## 1. Introduction

The emission of diesel engines due to the high content of particulate matter (PM) and to the presence of nitrogen oxides, among other pollutants, is harmful for the environment as well as for the human health [1]. In order to decrease the emission of particulate matter, catalytic filters in the exhaust pipe are frequently used. These filters must retain the soot, catalyze the combustion emissions and regenerate continuously.

There exist numerous reports of formulations able to decrease the soot combustion temperature from high temperatures (about 600 °C) up to the temperatures of gases in an exhaust pipe [2–6].

The different proposed mechanistic hypotheses are based on the following catalyst properties: the capacity to store oxygen [7], the increase of the contact between the soot (solid) and the catalyst (solid) [8,9], the presence of systems with redox functions [10–13]. Likewise, this type of materials must fulfill the need of being stable and active in atmospheres similar to that ones present in the exhaust pipe.

Catalysts containing compounds of alkaline metals (potassium, lithium, sodium and cesium) are particularly active, being potassium the most studied element of group 1 [14–19].

Some of these catalysts are used as molten salts and others are based on the use of supported salts. The stability of this last type of catalysts is based on the salt-support interaction. The anion nature of the alkaline metal salt has influence on the catalyst activity, and it has been observed that catalysts prepared using nitrates present higher activities than other precursors. Besides, it was found that among supported alkaline nitrates, cesium nitrate is the most active [12,17].

In previous works, it was possible to notice by means of spectroscopic techniques that catalysts containing nitrates can oxidize the soot so being reduced to nitrite [10]. This working hypothesis is accepted and other authors postulate the activity of nitrate anions.

Some authors propose the decomposition of bulk cesium nitrate into oxides and peroxides and they suggest, for the supported cesium nitrate, that part of cesium nitrate remains on the catalytic surface [15]. Catalysts containing only alkaline nitrates present a disadvantage, they do not present total selectivity to $CO_2$ and it is necessary to add transition metals able to oxidize the generated CO. In recent works, it has been reported that catalysts that have gold in their formulations are active for CO oxidation [20–23]. In this respect, it is interesting the use of catalysts promoted with gold for the complete soot combustion. The selection of this metal is based on the fact that it is cheaper and more plentiful than the other precious metals, [24]. On the other hand, there exist publications indicating that Au-based catalysts present activity for the reaction of $NO_x$ reduction [25].

The aim of this work is the study of $CsNO_3$ and gold-based catalysis for the diesel soot combustion reaction in presence of $O_2$/inert and $NO/O_2$/inert. Furthermore, several characterization techniques

* Corresponding author. Fax: +54 221 4211353.
*E-mail address:* eponzi@quimica.unlp.edu.ar (E.N. Ponzi).

0926-860X/$ – see front matter © 2010 Elsevier B.V. All rights reserved.
doi:10.1016/j.apcata.2010.10.024

have been performed to study the nature of gold and cesium nitrate in these catalysts.

## 2. Experimental

### 2.1. Preparation and characterization of catalysts

Hydrated zirconium oxide ($ZrO_2{\cdot}nH_2O$) was obtained by hydrolysis of zirconium oxychloride, $ZrOCl_2{\cdot}6H_2O$ (Fluka). The necessary amount of aqueous ammonia (Tetrahedron 28%) was added to the zirconium oxychloride to reach a pH 10. The product obtained by hydrolysis was filtered and washed until it was free from chloride ions, as determined by the silver nitrate test. The hydrated zirconium oxide ($ZrO_2{\cdot}nH_2O$) thus obtained was dried at 80 °C for 24 h. This solid was then milled in a mortar and sieved to obtain particle sizes between 0.150 and 0.090 mm. The other supports, $ZrO_2$ and $SiO_2$, are commercial products provided by Anedra and Degussa, respectively.

For the preparation of catalysts with cesium nitrate, the impregnation of supports was carried out with an aqueous solution of cesium nitrate, in a rota-vapor equipment at 100 °C, rate 170 rpm and a vacuum pressure of 500 mm Hg. The obtained solids were dried for 2 h at 80 °C. Catalysts containing cesium nitrate and gold were prepared by impregnation of supports with an aqueous solution of cesium nitrate as it was described above and, after the drying step, the impregnation with a solution $HAuCl_4{\cdot}3H_2O$ (1.0 wt% of Au) was performed. Catalysts containing cesium nitrate and gold were prepared by impregnation of supports with an aqueous solution of cesium nitrate as it was described above. With supports of $ZrO_2{\cdot}nH_2O$ and $ZrO_2$, successive gold impregnations were made with intermediate drying. Meanwhile, for the $SiO_2$ support, the impregnation with Au was made with a more diluted solution to produce a better solid wetting. This same impregnation method was used for the preparation of catalysts Au/supports. Precursors were prepared with a nominal concentration of 23.6% in weight of cesium nitrate and 2.0% in weight of Au. These precursors were calcined at 600 °C for 1 h.

The temperature selected for calcination of precursors was 600 °C, approximately 200 °C above the operation temperature of catalysts in an exhaust pipe. This calcination temperature assures no catalyst transformations during activity measurements. In order to differentiate zirconia supports, the catalyst impregnated on $ZrO_2$ will be named Z and the catalyst prepared by impregnation of $ZrO_2{\cdot}nH_2O$, Zt. The silica will be named S. In this way, catalysts with cesium nitrate will be named $CsNO_3Z$, $CsNO_3Zt$ and $CsNO_3S$, gold catalysts will be named AuZ, AuZt and AuS and those ones with both species will be $CsNO_3AuZ$, $CsNO_3AuZt$ and $CsNO_3AuS$.

### 2.2. Characterization of catalysts

Specific surface areas of support and catalysts were determined by the BET method using $N_2$ adsorption isotherm; the nitrogen adsorption isotherm was evaluated by using an automated Micromeritics ASAP 2020 equipment. Pore specific volume of materials was determined.

Bulk gold and cesium contents were determined by atomic absorption spectrophotometry with a spectrophotometer PerkinElmer AA 3110.

The content of soluble nitrate ions was determined by means of a photometric method with a colorimeter DR/890 Hatch. For this, samples were washed with distilled water and nitrates in washing waters were analyzed.

The elemental nitrogen content was determined by means of elemental analysis (EA) with a CHNS LECO 932 analyzer.

Crystalline phases within the catalysts were identified by powder X-ray diffraction (XRD) analysis using a Rigaku D-Max III diffractometer equipped with Ni-filtered Cu Kα radiation (λ = 1.5378 Å).

The melting point of the potassium nitrate in the catalysts was studied by differential scanning calorimetry (DSC) using a Shimadzu DSC 50 equipment. α-$Al_2O_3$ was used as reference and $N_2$ as a carrier.

The presence of nitrate anions on fresh and used catalysts was studied by means of FTIR spectroscopy using a Bruker EXINOX 55 equipment. Spectra were recorded at room temperature in the 4000–400 $cm^{-1}$ range and the samples were prepared in form of discs with KBr.

The X-ray photoelectron spectroscopy (XPS) was performed with a Physical Electronics PHI-5700 spectrometer, equipped with a dual X-ray source of Mg-Kα (1253.6 eV) and Al-Kα (1486.6 eV) and a multi-channel detector. Spectra of powdered samples were recorded in the constant pass energy mode at 29.35 eV, using a 720 μm diameter analysis area. Charge referencing was measured against adventitious carbon (C 1s at 284.8 eV). A PHI ACCESS ESCA-V6.0 F software package was used for acquisition and data analysis. A Shirley-type background was subtracted from the signals. Recorded spectra were always fitted using Gaussian–Lorentzian curves in order to determine the binding energy of the different element core levels more accurately.

TPR (temperature programmed reduction) experiments were carried out with the conventional equipment. The TPR was performed using 10% hydrogen in nitrogen (flow rate 20 $cm^3\,min^{-1}$) with a heating rate of 10 °C/min up to 950 °C. The sample loaded was 20 mg.

Experiments of precursor decomposition were made using a reactor with programmed temperature with mass detector (Dycor System 2000) in order to detect all gaseous sub-products.

### 2.3. Measurements of catalytic activity

Thermal programmed oxidation techniques were used to carry out the catalytic tests. Two types of catalytic experiments were carried out: exploratory runs in a thermogravimetric reactor with an air/He feed and experiments in a fixed bed reactor with $NO/O_2/He$ feed. Experiments in a thermogravimetric reactor are fast and exploratory and the aim is to know if catalysts present activity in oxygen presence, while experiments in the flow reactor are performed in order to investigate the influence of the NO presence in the activity. Besides, in the flow reactor a poor contact (loose contact) is used to approach to the real contact conditions.

In the first case, the soot combustion was performed in a thermobalance (TGA-50 Shimadzu) with a heating rate of 10 °C/min and an air/He feed (2:1). The soot sample used in this work is a synthetic flame soot named Printex-U manufactured by Degussa. In order to carry out activity experiments, the soot (3 mg) and the catalyst (30 mg) were milled carefully in an agate mortar before introduction into the reactor. The weight loss and the temperature were recorded as a function of time. The derivative curve (DTGA) was obtained from the weight loss information as a function of time, and from this curve the temperature where the combustion rate is maximum ($T_{max}$).

In the second case, catalytic tests in $O_2/NO/He$ presence were performed in a temperature programmed oxidation (TPO) apparatus, a fixed bed quartz microreactor with analysis of reaction gases. The microreactor was electrically heated with a heating rate of 2 °C/min. The reaction mixture was obtained from three feed lines individually controlled: NO/He, $O_2$/He, and He to close the balance. The reactor was fed with the following mixture: 1500 ppm of NO and 8% of $O_2$ (Q total = 50 ml/min). The microreactor was loaded with 30 mg of catalyst and 3 mg of soot (Printex-U) and the

**Table 1**
BET surface areas of supports and of $CsNO_3$/oxide catalysts.

| Support | Area ($m^2$/g) | Support pore specific volume ($cm^3\ g^{-1}$) | Area of Cs catalysts | Catalysts pore specific volume ($cm^3\ g^{-1}$) |
|---|---|---|---|---|
| $SiO_2$ | 200 | 0.183 | 75.5 | 0.069 |
| $ZrO_2{\cdot}nH_2O$ | 320 | 0.210 | – | – |
| $ZrO_2{\cdot}nH_2O$ calc600 | 60 | 0.109 | 5.6 | 0.009 |
| $ZrO_2$ monoclinic | 8 | 0.005 | 0.5 | 0.001 |

combustion was carried out in the range of 200–650 °C. Before the reaction, the soot was mixed with the catalyst, with a spatula (loose contact). Reaction products were monitored with a gas chromatograph, Shimadzu model GC-8A, provided with a TCD detector. The sampling was carried out approximately every 8 min. The separation of products was performed with a concentric column CTRI of Alltech. This system permitted the identification and quantification of the peaks of $O_2$, $N_2$, $CO_2$, and CO. The concentration of $CO_2$ and CO was determined from the area of $CO_2$ and CO peaks obtained by chromatographic analysis.

## 3. Results and discussion

### 3.1. Characterization of catalysts

#### 3.1.1. Surface area and chemical analysis

Catalysts were prepared using oxidic supports, $ZrO_2$, $ZrO_2{\cdot}nH_2O$ and $SiO_2$, whose specific surface varies significantly. The BET areas and pore specific volume of supports and of the series of catalysts $CsNO_3$/support, previously calcined at 600 °C for 2 h, were determined (Table 1). The obtained results indicate that catalysts present lower BET areas than those of the corresponding supports and this is attributed to the fact that the cesium nitrate is a fundent that, when it is added on a support, decreases its area considerably. In the catalyst prepared from $ZrO_2{\cdot}nH_2O$, the area also diminishes by effect of support nucleation and crystallization. When calcining $ZrO_2{\cdot}nH_2O$ in cesium nitrate absence, a zirconia with a BET area of 60 $m^2$/g is obtained. In the $CsNO_3$ presence, the obtained BET area is 5.6 $m^2$/g, which indicates a strong material sinterization. This same effect is observed in catalysts prepared from commercial supports. The area decrease is attributed to the blocking of a large fraction of pores and the pore volume of catalysts with cesium nitrate is substantially lower than the pore volume of supports without impregnation.

Catalysts were formulated with the following nominal concentrations: 2.0% (w/w) gold, 16.1% (w/w) cesium, 7.5% (w/w) nitrate ion. Table 2 shows results of the concentration of gold and cesium (AAS), nitrogen (EA) and nitrate anion (colorimetric analysis).

In catalysts that only contain cesium nitrate supported on zirconia, $CsNO_3Z$ and $CsNO_3Zt$, the cesium nitrate concentration, estimated from the elemental nitrogen concentration, is near to the nominal value (23.6%), which would indicate that most of supported cesium nitrate has not been volatilized or decomposed in its respective oxides ($CsO_2$, $Cs_7O_2$). The same results appear from analyses of nitrate ion concentration determined by colorimetric analysis. In these catalysts, the cesium nitrate concentration estimated from the cesium content (AAS) is similar to the nominal one.

**Table 2**
Chemical compositions of the catalysts.

| | %$CsNO_3$[a] | %Au[b] | %$CsNO_3$[c] | %$CsNO_3$[d] |
|---|---|---|---|---|
| $CsNO_3S$ | 5.4 | | 19.8 | 4.0 |
| $CsNO_3Z$ | 24.2 | | 23.1 | 23.4 |
| $CsNO_3Zt$ | 24.4 | | 21.3 | 24.8 |
| AuS | | 1.5 | – | |
| AuZ | | 1.6 | – | |
| AuZt | | 2.7 | – | |
| $CsNO_3AuS$ | 0.1 | 1.0 | 18.7 | – |
| $CsNO_3AuZ$ | 4.0 | 0.8 | 20.9 | – |
| $CsNO_3AuZt$ | 1.3 | 2.3 | 23.8 | – |

[a] Estimated from % N determined by elemental analysis.
[b] By AAS.
[c] Estimated from %Cs (AAS).
[d] Estimated from %$NO_3$ (colorimetric).

The catalyst supported on silica, $CsNO_3S$, presents a different behavior. The cesium nitrate concentration (19.81% (w/w)) estimated from the cesium concentration is slightly lower than the nominal (23.6%), while the cesium nitrate concentration estimated from the nitrogen content and the colorimetric analysis is much lower than the nominal, which indicates that during precursor calcination, an important cesium portion remains in the catalyst as other species. It is evident that the anchoring of nitrate species in the silica is weak.

The gold concentration in AuZ and AuS catalysts is slightly lower to the nominal (2.0%) while it is higher in the AuZt catalyst. The concentration increase in AuZt is attributed to water loss of the support during precursor calcination and to an increase in the supported species concentration.

In catalysts containing cesium nitrate and gold, $CsNO_3AuZ$, $CsNO_3AuZt$ and $CsNO_3AuS$, the cesium nitrate concentration estimated from the nitrogen content is noticeably lower than the nominal (23.6%). This behavior differs from that observed in catalysts that only contain cesium nitrate. The cesium concentration obtained by AAS is similar to the nominal (16.5%), which indicates that the cesium nitrate has been transformed in other species during calcination of precursors that contain gold salt.

In order to analyze the nature of cesium and cesium nitrate species and to explain the differences between nominal and analyzed concentrations, studies of X-ray diffraction, DSC and FTIR were performed.

#### 3.1.2. X-ray diffraction

In the XRD diagrams of catalysts, AuZ, $CsNO_3Z$, and $CsNO_3AuZ$ (Fig. 1A), it is possible to detect diffraction lines typical of monoclinic zirconia ($2\theta = 28.2°$, 31.5° and 34.5°), of cesium nitrate C and of metallic gold ($2\theta = 38.2°$ and 44.5°).

In the XRD diagrams of catalysts $CsNO_3Z$ and $CsNO_3AuZ$, the most intense signal of cesium nitrate at 28.28° is overlapped with a diffraction line of the support but the other signals are observed. The $CsNO_3AuZ$ catalyst presents these signals with lower intensity than the $CsNO_3Z$ in agreement with the cesium nitrate decrease observed by chemical analyses.

The XRD diagram of the AuZ catalyst presents diffraction lines associated to metallic gold and these signals are less evident in the XRD diagram of $CsNO_3AuZ$. This can be the result of a low gold concentration as found by AAS.

Also, signals associated to the presence of CsCl ($2\theta = 30.6°$ and 21.55°) are observed in the diagram of $CsNO_3AuZ$ catalyst. These results sustain the hypothesis of cesium nitrate decomposition in other species during the calcination stage. It is possible that cesium nitrate dissolves during the second impregnation and forms CsCl that precipitates. The presence of cesium chloride may be due to this dissolution and precipitation in presence of chlorides during the second impregnation or by a chemical reaction between gold salt and cesium nitrate. However, signals associated to the presence

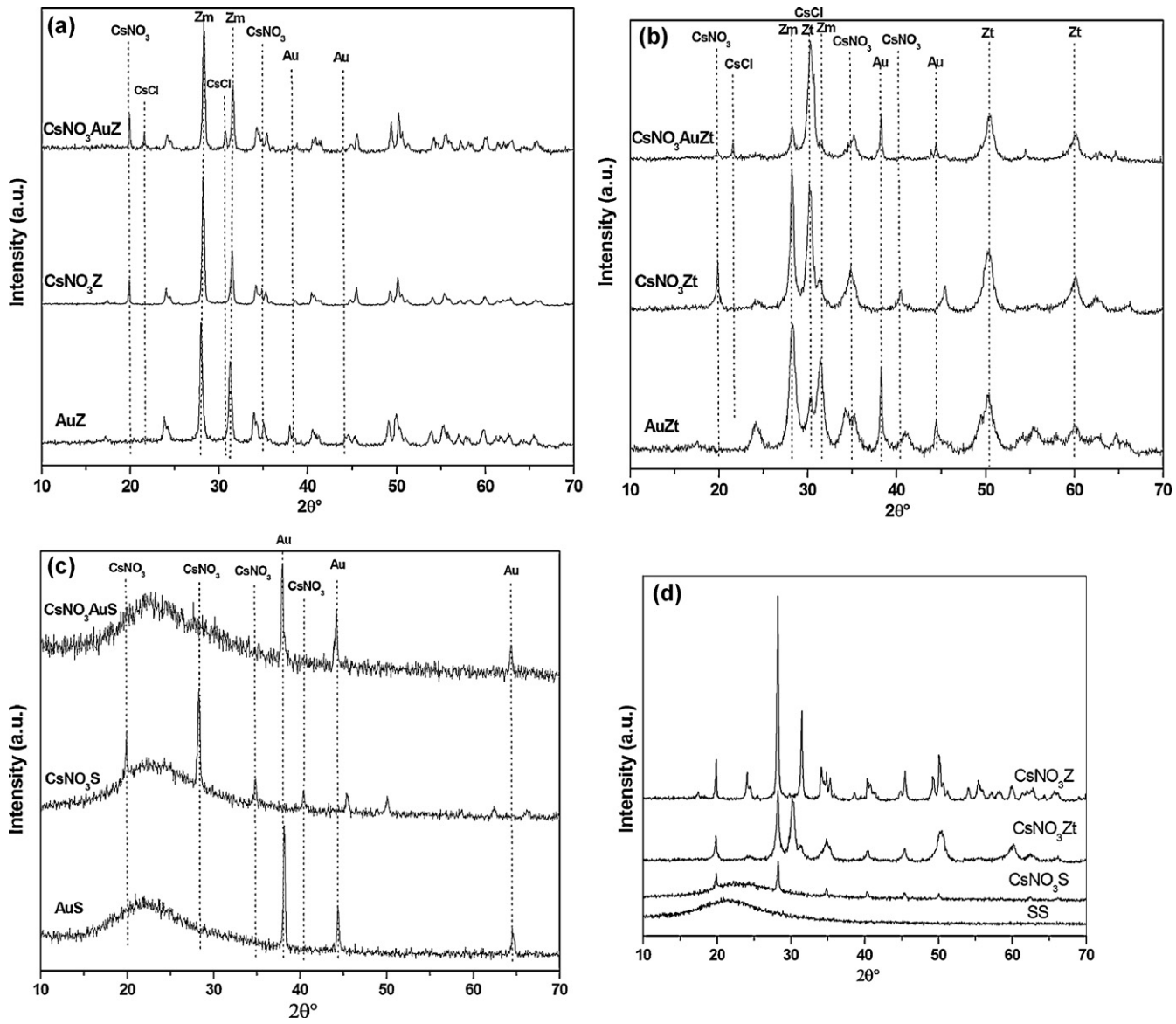


**Fig. 1.** (A) XRD diagrams of catalysts supported on monoclinic zirconia ($ZrO_2$). Zm is monoclinic zirconia. (B) XRD diagrams of catalysts supported on $ZrO_2{\cdot}nH_2O$. Zm is monoclinic zirconia and Zt is tetragonal zirconia. (C) XRD diagrams of catalysts supported on silica. (D) XRD diagrams of $CsNO_3$/support catalysts. SS: Silica support.

of $AuCl_3$ ($2\theta = 16.62^\circ$, $33.61^\circ$, $31.37^\circ$ and $43.23^\circ$) or oxidic cesium species ($CsO_2$, $Cs_7O_2$, $Cs_2O$, etc.) are not observed.

Fig. 1B shows XRD diagrams of catalysts $CsNO_3Zt$, $CsNO_3AuZt$ and AuZt. During calcination, the amorphous $ZrO_2{\cdot}nH_2O$ support crystallizes in different polymorphisms depending on the nature of the host cation. Catalysts $CsNO_3Zt$ and $CsNO_3AuZt$ adopt a tetragonal metastable structure ($2\theta = 30.5^\circ$, $35.2^\circ$ and $50.7^\circ$). Instead, in the AuZt catalyst, the predominant zirconia phase is the monoclinic ($2\theta = 28.2^\circ$, $31.5^\circ$ and $34.5^\circ$). These results suggest a possible interaction between cesium ions and the zirconium oxide originated during calcination of $ZrO_2{\cdot}nH_2O$ in alkaline ion presence, generating a $Zr^{+4}$ substitution and the generation of oxygen vacancies. This fact has been also observed by other authors [26,27].

In diagrams of catalysts $CsNO_3Zt$ and $CsNO_3AuZt$, it is possible to observe signals associated to the presence of crystalline $CsNO_3$ and these signals are more intense in the diffractogram of the $CsNO_3Zt$ catalyst. These results agree with those found by chemical analysis, which show a significant difference in the cesium nitrate concentration of both catalysts.

Catalysts AuZt and $CsNO_3AuZt$ present diffraction lines associated to metallic gold at $2\theta = 38.2^\circ$ and $44.5^\circ$.

Fig. 1C shows XRD diagrams of catalysts AuS, $CsNO_3S$ and $CsNO_3AuS$. XRD lines of $CsNO_3$ can be observed only in the $CsNO_3S$ catalysts. Results achieved agree with that found by chemical analyses that show a very low cesium nitrate concentration in the $CsNO_3AuS$ catalyst.

Catalysts AuS and $CsNO_3AuS$ show diffraction lines of metallic gold and these signals are more intense in the AuS catalyst.

When comparing the intensity of the diffraction line at $19.80^\circ$ ($CsNO_3$) in diagrams of catalysts $CsNO_3Z$, $CsNO_3Zt$ and $CsNO_3S$, it is possible to observe that the signal is more intense in $CsNO_3Z$ (Fig. 1D). This catalyst contains a high $CsNO_3$ content and a very low surface area. The formation of large $CsNO_3$ crystals is suggested. During the calcination step, the salt melts and blocks a large fraction of pores generating a segregation of $CsNO_3$ crystals. This fact is evidenced with the drastic decrease of the specific surface and the smaller pore size found in these catalysts.

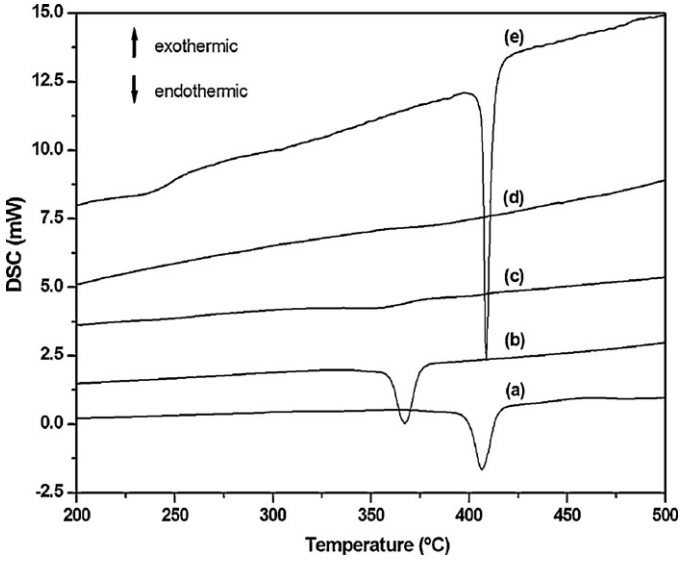


**Fig. 2.** DSC diagram of $CsNO_3$/support catalysts and $CsNO_3$ salt: (a) $CsNO_3Z$, (b) $CsNO_3AuZ$, (c) $CsNO_3Zt$, (d) $CsNO_3S$, (e) $CsNO_3$. Catalyst mass: 10 mg, $CsNO_3$ mass: 2.36 mg.

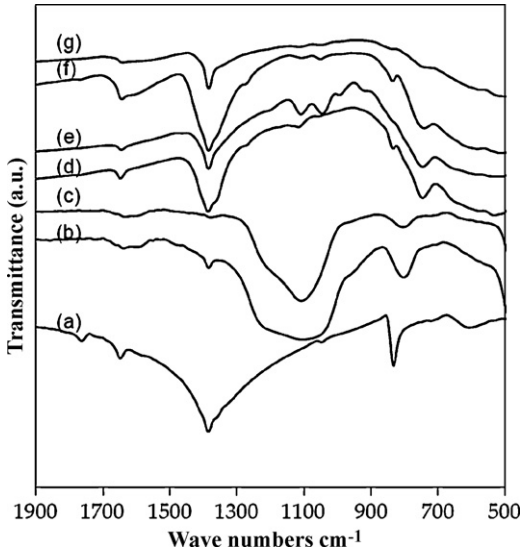


**Fig. 3.** FTIR spectra of $CsNO_3$ bulk and catalysts: (a) $CsNO_3$, (b) $CsNO_3S$, (c) $CsNO_3AuS$, (d) $CsNO_3Z$, (e) $CsNO_3AuZ$, (f) $CsNO_3Zt$, (g) $CsNO_3Au$ Zt.

### 3.1.3. Differential scanning calorimetry, DSC

Fig. 2 shows DSC diagrams of catalysts $CsNO_3$/support and of bulk cesium nitrate.

The DSC diagram of $CsNO_3$ shows an endothermic signal centered at 405 °C assigned to salt melting. The DSC diagram of $CsNO_3Z$ catalyst shows clearly this signal, evidencing the presence of big crystallites of $CsNO_3$. The diagram of the $CsNO_3Zt$ catalyst shows a weak endothermal signal at 360 °C. This signal is attributed to the melting of $CsNO_3$ that it is much dispersed. In the DSC diagram, the $CsNO_3S$ catalyst does not show signals of salt melting, even when the diffraction lines of cesium nitrate are clearly observed by XRD. These results can be correlated with the values of surface area and cesium nitrate concentration, the $CsNO_3Z$ catalyst is prepared on a low surface area support, it presents high cesium nitrate concentration which leads to a poor dispersion of supported salt and a very clear melting signal.

From the series of catalysts $CsNO_3$AuSupport, the only catalyst that presents an evident melting signal is the $CsNO_3AuZ$ catalyst.

### 3.1.4. Infrared spectroscopy (FTIR)

Fig. 3 shows the FTIR spectra of cesium containing catalysts. The FTIR spectrum of cesium nitrate salt presents a band at 1385 $cm^{-1}$ associated to the antisymmetric N–O stretching vibration mode ($\nu_{as}$). Besides it is possible to note a weak band at 1050 $cm^{-1}$ associated to the symmetric vibration mode ($\nu_s$) and the band associated to the angular deformation O–N–O at 830 $cm^{-1}$.

In spectra of catalysts $CsNO_3Zt$, $CsNO_3Z$ and $CsNO_3S$, an absorption band at 1385 $cm^{-1}$ assigned to antisymmetric N–O stretching of free nitrate species is observed. This band is accompanied with the band of the angular deformation O–N–O at 830 $cm^{-1}$ [28]. This last one cannot be observed in the spectrum of $CsNO_3S$ catalyst because it is overlapped with the support absorption bands.

The band associated to antisymmetric N–O stretching (1385 $cm^{-1}$) is present in spectra of catalysts $CsNO_3AuZ$ and $CsNO_3AuZt$. In this series, the signals are weaker than the ones observed in spectra of series $CsNO_3$Support. In the spectrum of $CsNO_3AuS$ catalyst, no absorption bands associated to the presence of nitrate ions are observed. This fact agrees with XRD results where no diffraction lines of the supported salt are observed.

It is not possible to observe, in any spectrum, FTIR signals associated to the presence of monodentate and bidentate nitrate species, which are evidenced with antisymmetric N–O stretching bands placed at 1420 and 1500 $cm^{-1}$.

### 3.1.5. Photoelectron spectroscopy (XPS)

Fig. 4A shows XPS spectra for the Cs $3d_{5/2}$ region of supported $CsNO_3$ catalysts, Fig. 4B shows XPS spectra for the Au $4f_{7/2}$ region of the series of supported Au catalysts, and Fig. 4C shows XPS spectra for the Au $4f_{7/2}$ region of the series of supported $CsNO_3Au$ catalysts. The signal attributed to the presence of nitrates could not be observed, probably due to the nitrate ion decomposition by X-ray radiation. Other authors have reported the same phenomena when studied the degradation of nitrates due to the fact that several compounds can be damaged by X-ray radiation [29].

The position of the emission band was determined from spectra and the analysis of the superficial cesium concentration was carried out. Data attained are presented in Table 3.

A high cesium concentration is found on the surface of catalysts supported on zirconia. It is also possible to observe that when adding Au the surface cesium concentration is not modified.

The Au $4f_{7/2}$ signal is observed in all catalysts with Au at 83.9 eV. This signal is assigned to metallic Au and photoemissions at 85.7 eV are not observed. This is the value found in the literature for $Au_2O_3$ [30]. Results obtained by XPS are in agreement with those obtained by XRD and reject the possibility that a small portion of superficial gold is found as oxidic phases.

The surface gold concentration in catalysts $CsNO_3AuZ$ and $CsNO_3AuZt$ is lower than that observed in the case of AuZ and AuZt catalysts. Probably, in these catalysts, part of gold is found covered by cesium nitrate. Instead, the surface gold concentration in the $CsNO_3AuS$ catalyst is higher than that observed in the AuS catalyst.

**Table 3**
Surface concentrations and cesium BE in catalysts.

| Sample | [Au] (%) | [Cs] (%) | Cs BE | Au $4f_{7/2}$ |
|---|---|---|---|---|
| $CsNO_3S$ | – | 17.29 | 725.0 | – |
| $CsNO_3Z$ | – | 24.40 | 724.4 | – |
| $CsNO_3Zt$ | – | 18.30 | 724.2 | – |
| AuS | 0.10 | – | – | 83.2 |
| AuZ | 3.43 | – | – | 84.1 |
| AuZt | 7.38 | – | – | 83.6 |
| $CsNO_3AuS$ | 0.83 | 18.08 | 724.9 | 82.9 |
| $CsNO_3AuZ$ | 0.60 | 21.58 | 724.2 | 82.6 |
| $CsNO_3AuZt$ | 3.38 | 22.75 | 724.3 | 84.0 |

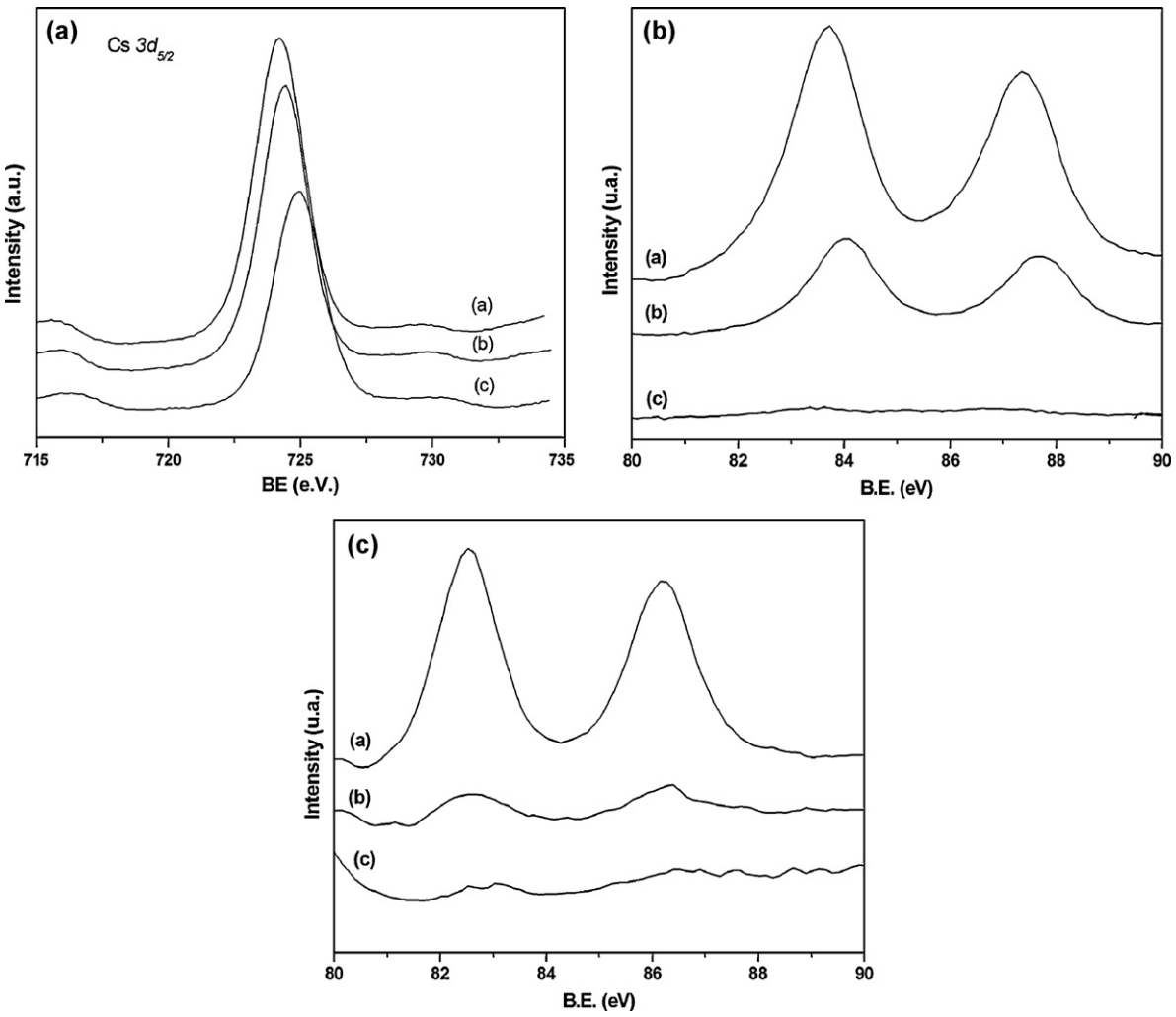


**Fig. 4.** (A) X-ray photoelectron spectra for the Cs $3d_{5/2}$ region: (a) $CsNO_3Zt$, (b) $CsNO_3Z$ and (c) $CsNO_3S$. (B) X-ray photoelectron spectra for the Au 4*f* region: (a) AuZt, (b) AuZ, (c) AuS. (C) X-ray photoelectron spectra for the Au 4*f* region: (a) $CsNO_3AuZt$, (b) $CsNO_3AuZ$, (c) $CsNO_3AuS$.

*3.1.6. Temperature programmed reduction with $H_2$ (TPR)*

The reducibility of species present in series of supported $CsNO_3$ and $CsNO_3Au$ catalysts is evaluated by means of the hydrogen temperature programmed reduction technique. No reduction of gold species is expected because in all cases there is metallic gold as it was noticed by XPS.

In TPR profiles of $CsNO_3$ catalysts (Fig. 5A–C), the reduction signal starts around 500 °C and it is centered at 580 °C for catalysts supported on zirconia, $CsNO_3Z$ and $CsNO_3Zt$, and at a higher temperature (630 °C) for the catalyst supported on silica, $CsNO_3S$. This reduction signal is attributed to the reduction of nitrate species [31]. The nitrate ion reduction is performed slowly in the catalyst supported on silica evidencing higher supported salt interaction. This indicates that the remainder nitrate portion stays in the catalyst with high interaction degree. Catalysts that show higher hydrogen consumption are $CsNO_3Z$ and $CsNO_3Zt$. The catalyst that shows lower hydrogen consumption is the $CsNO_3S$ catalyst, which is the one that contains lower nitrate ion concentration. These results corroborate that the nitrate concentration in catalysts supported on zirconia is several times higher than the one found in the catalyst supported on silica.

The hydrogen consumption of supported $CsNO_3Au$ catalysts is substantially lower than that observed in the case $CsNO_3$ catalysts due to lower nitrate concentration. The TPR diagram of $CsNO_3AuS$ catalyst does not show any reduction signal, this result is in agreement with the very low concentration of cesium nitrate.

The nitrate reduction peaks in catalysts $CsNO_3AuZt$ and $CsNO_3AuZ$ present the maxima at lower temperatures than catalysts without gold promotion. The temperature of maxima is between 530 and 540 °C, respectively, while for catalyst $CsNO_3Zt$ and $CsNO_3Z$ the same peaks are found at 585 and 574 °C. These experiments show clearly an influence of gold in nitrate reduction in catalysts supported on zirconia. Probably, the $H_2$ is absorbed and dissociates on the metallic particles and it spilled-over to nitrate ions placed near them.

Results obtained from different characterization techniques are analyzed in the following paragraphs. Results obtained by FTIR are in agreement with the ones achieved according to chemical analysis and X-ray diffraction, XPS and TPR, where it was possible to note that the cesium nitrate concentration is low in catalysts containing gold in their composition. This fact is accompanied by the appearance of a peak in the XRD diffractogram of $AuCsNO_3$ catalysts assigned to CsCl. A probable mechanism is that gold salt decomposes giving molecular chlorine through reaction 1 which is thermodynamically feasible from 300 °C (Table 4), and the generated $Cl_2$ may attack the cesium nitrate according to reaction 2 being the CsCl a product of this reaction. The mass detector on-line during the calcination of precursor $AuCsNO_3$Support corroborated the presence of $NO_2$ ($m/z$ = 30 and 46).

$$2AuCl_3 = 2Au^0 + 3Cl_2(g) \quad (1)$$

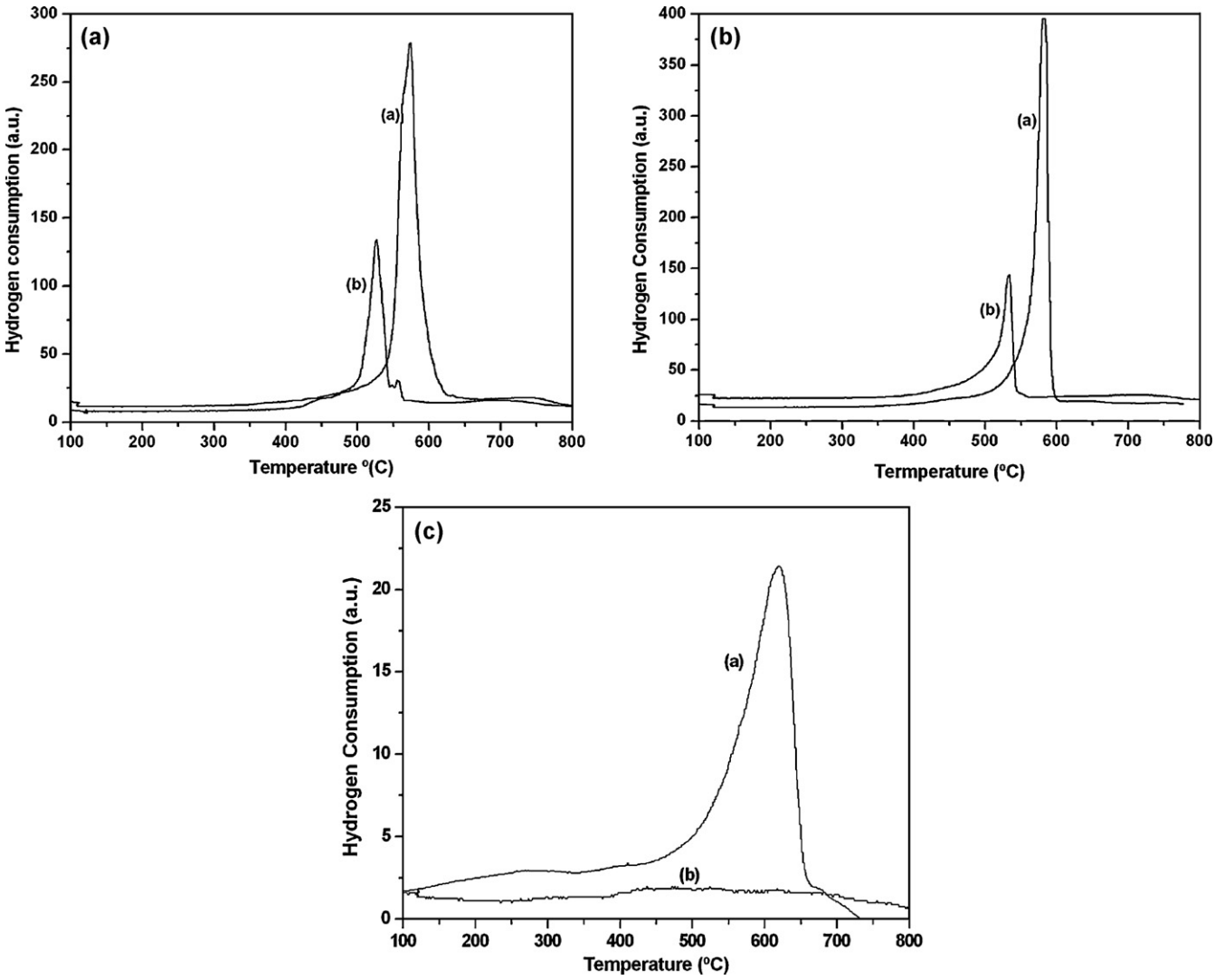


**Fig. 5.** (A) TPR of catalysts: (a) $CsNO_3Z$ and (b) $CsNO_3AuZ$. (B) TPR of catalysts: (a) $CsNO_3Zt$ and (b) $CsNO_3Au$ Zt. (C) TPR of catalysts: (a) $CsNO_3S$ and (b) $CsNO_3AuS$.

$$Cl_2(g) + 2\,CsNO_3 = 2\,CsCl + O_2(g) + 2\,NO_2(g) \quad (2)$$

For this reason, a series of catalysts was prepared where thermal treatments performed to precursors were modified. This new series was prepared by support impregnation with gold salt followed by an intermediate calcination at 600 °C. Then, an impregnation with cesium nitrate was made and the obtained material was calcined at 600 °C. So, the attack of molecular chlorine to cesium nitrate is avoided.

Fig. 6 shows XRD diagrams of catalysts prepared by modifying the preparation method, $CsNO_3Au(c)Z$, $CsNO_3Au(c)Z$ and $CsNO_3Au(c)S$. XRD diagrams differ significantly from the ones obtained with the original preparation technique. New catalysts do not present X-ray diffraction lines of CsCl salt and they continue

**Table 4**
Gibbs free energies for reactions (1) and (2).

| Temperature (°C) | $\Delta G$ reaction (1) (kJ) | $\Delta G$ reaction (2) (kJ) |
|---|---|---|
| 100 | 74.7 | 60.7 |
| 200 | 32.9 | 26.9 |
| 300 | −7.5 | −4.4 |
| 400 | −46.8 | −34.4 |
| 500 | −85.1 | −59.9 |
| 600 | −122.2 | −84.1 |

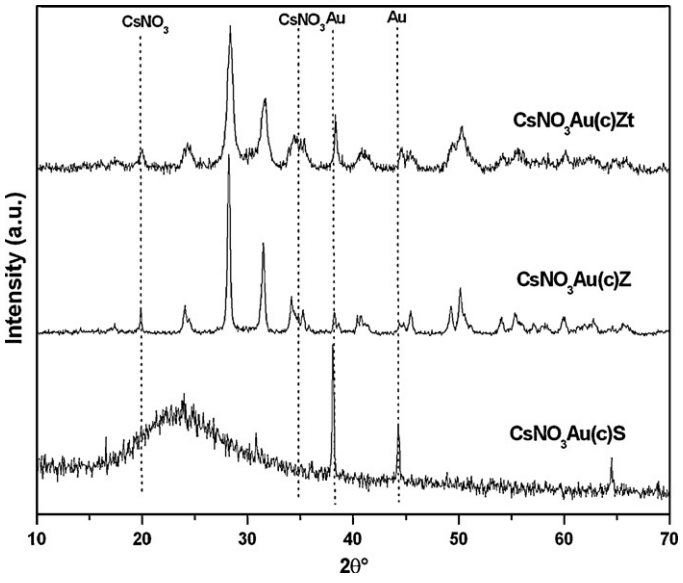


**Fig. 6.** XRD diagrams of $CsNO_3Au(c)$/support catalysts.

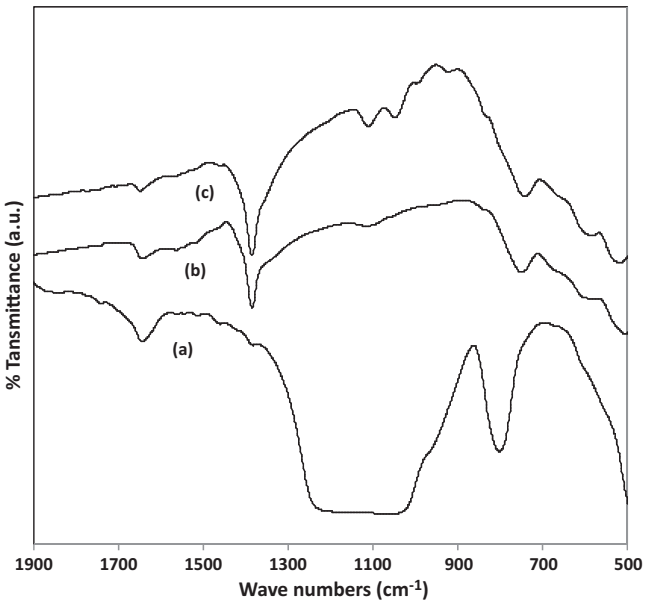


**Fig. 7.** FTIR spectra of $CsNO_3Au(c)$/support catalysts: (a) $CsNO_3Au(c)S$, (b) $CsNO_3Au(c)Zt$, (c) $CsNO_3Au(c)Z$.

presenting diffraction lines of $CsNO_3$ ($2\theta = 38.2^\circ$ and $44.5^\circ$) and of metallic gold ($2\theta = 38.2^\circ$ and $44.5^\circ$). The presence of nitrate anions can be also observed by means of FTIR spectroscopy in the three catalysts. Spectra show the typical signal of antisymmetric vibration of the N–O bond of free nitrate ions at 1385 $cm^{-1}$ (Fig. 7) and these signals are more intense than the ones found with the series $AuCsNO_3$support, fundamentally in the $CsNO_3Au(c)/S$ catalyst. In the spectrum of $CsNO_3AuS$ catalyst, this signal was not evidenced.

### 3.2. Measurements of catalytic activity

#### 3.2.1. Catalytic results obtained in a thermogravimetric reactor in air/He presence

Fig. 8A and B shows catalytic results obtained in the thermogravimetric reactor. Table 5 presents temperatures obtained when performing TPO tests in presence and absence of catalysts, the initial reaction temperature ($T_i$), the maximum combustion rate temperature ($T_{max}$) and the temperature at which the reaction ends ($T_{final}$) are shown.

Supported gold catalysts Au/support present a poor activity in air/He presence. These results indicate that gold contributes very little to the activity of catalysts in this atmosphere.

Fig. 8A shows TPO diagrams achieved by using the series of supported $CsNO_3$ catalysts. In all cases the combustion of soot occurs at much lower temperatures than that of the pure soot (625 °C). The

**Table 5**
Catalytic results obtained in a thermogravimetric reactor fed with air/He with tight contact and high heating rate (10 °C/min).

| | $T_i$ | $T_{max}$ | $T_{final}$ |
|---|---|---|---|
| AuS | 430 | 585 | 620 |
| AuZ | 455 | 610 | 669 |
| AuZt | 430 | 598 | 643 |
| $CsNO_3S$ | 325 | 393 | 455 |
| $CsNO_3Z$ | 325 | 382 | 427 |
| $CsNO_3Zt$ | 325 | 393 | 430 |
| $CsNO_3AuS$ | 328 | 427 | 508 |
| $CsNO_3AuZ$ | 322 | 377 | 415 |
| $CsNO_3AuZt$ | 334 | 387 | 427 |
| $CsNO_3Au(c)S$ | 316 | 408 | 470 |
| $CsNO_3Au(c)Z$ | 321 | 373 | 416 |
| $CsNO_3Au(c)Zt$ | 323 | 380 | 423 |

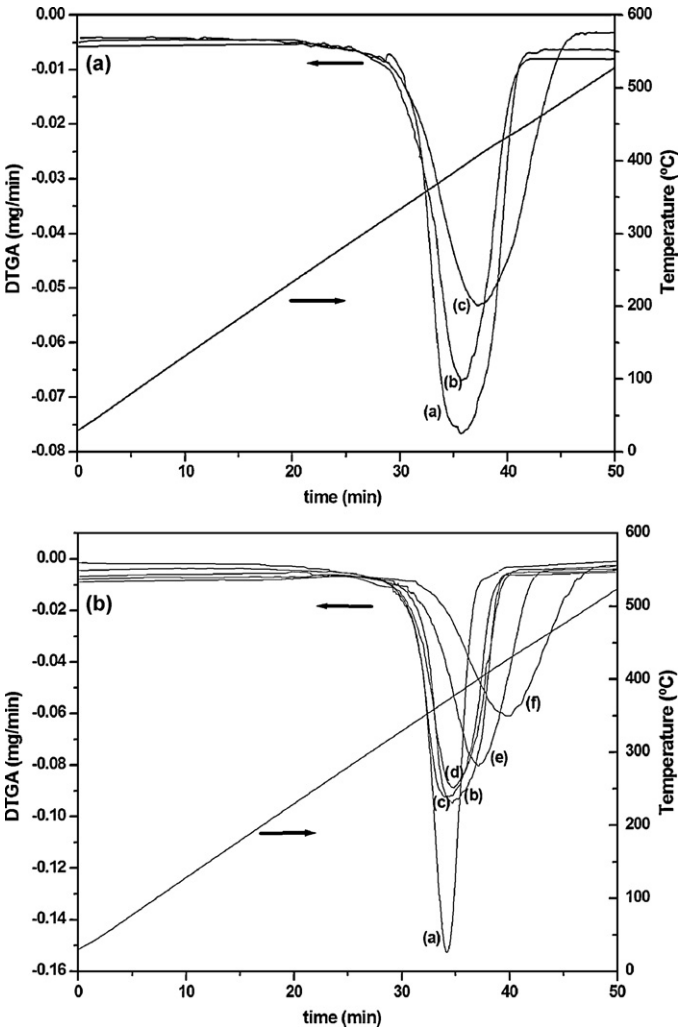


**Fig. 8.** (A) TPO of particulate matter (soot) with $CsNO_3$/support catalysts in air/He presence: (a) $CsNO_3Z$, (b) $CsNO_3Zt$, (c) $CsNO_3S$, (d) soot. (B) TPO of particulate matter (soot) with $CsNO_3Au$/Support and $CsNO_3Au(c)$/support catalysts in air/He presence: (a) $CsNO_3Au(c)Z$, (b) $CsNO_3AuZ$, (c) $CsNO_3Au(c)Zt$, (d) $CsNO_3AuZt$, (e) $CsNO_3Au(c)S$, (f) $CsNO_3AuS$.

three catalysts start with their combustion at a temperature near 325 °C and the combustion occurs at lower temperature in the case of $CsNO_3Z$ catalyst.

Data obtained by means of characterization techniques show that the more active catalysts, the $CsNO_3Z$, presents a high cesium nitrate concentration, the highest crystalline size observed by XRD, fusion signal evidenced by DSC, and high surface cesium concentration by XPS.

D. Hleis et al. [12] found similar catalytic results with a catalyst of cesium nitrate (15.11 cesium weight ratio (%)) supported over a monoclinic zirconia. The catalyst was obtained by impregnation of an amorphous zirconia prepared from $ZrO_2 \cdot nH_2O$ calcined at 300 °C. In this catalyst, the alkaline cation does not stabilize the zirconia metastable tetragonal phase. The catalyst prepared by Hleis et al. and the most active of the series $CsNO_3$Support, the $CsNO_3Z$, present reducible phases by hydrogen, free nitrate ions as predominant species (determined by FTIR) and a high amount of supported crystal $CsNO_3$ phase.

The soot oxidation is proposed as reaction mechanism by nitrate ion reduction [10–11,17]

$$2\,NO_3^- + C = 2\,NO_2^- + CO_2 \quad (3)$$

$$2\,NO_2^- + O_2 = 2\,NO_3^- \quad (4)$$

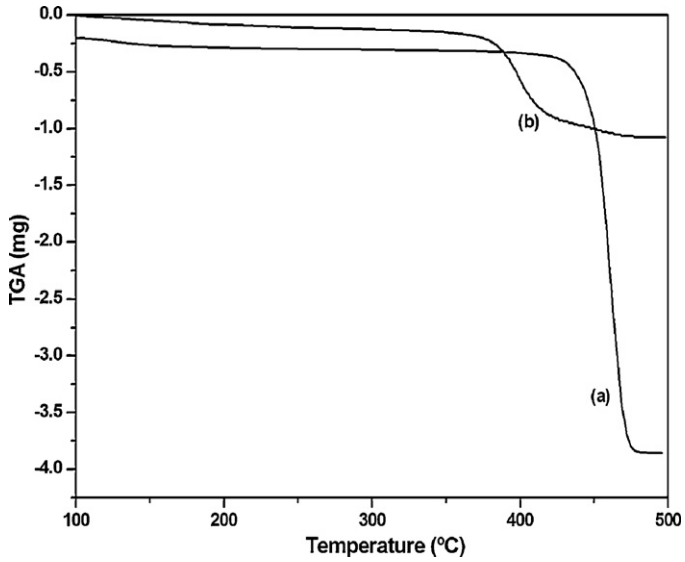


**Fig. 9.** TGA curves of a mixture of $CsNO_3$ and soot: (a) Helio (soot: 1 mg, $CsNO_3$: 25 mg), (b) Air/Helio (soot:1 mg; $CsNO_3$: 2 mg).

Physicochemical properties support the proposed model that supposes: (a) well contact soot–catalyst and (b) high nitrate ion concentration. The most active catalyst of the series, the $CsNO_3Z$ sample, presents both characteristics.

Fig. 9 shows TGA curves of a mixture of $CsNO_3$ and soot carefully milled in a mortar. The mass loss obtained in the experiment with helium atmosphere (a) is 3.54 mg for 1 mg soot. The theoretical mass loss by the reaction (3) is 3.66 mg per mg of soot. The nitrite cannot be regenerated to nitrate since there is no oxygen in the flow that feeds to the thermobalance.

The mass loss obtained in the experiment with an atmosphere air/helium is 0.94 mg per mg of soot. The mass loss only corresponds to soot. This result suggests that nitrate intervenes in the catalytic cycle being regenerated with the oxygen of the gaseous current.

Fig. 10 shows FTIR spectra of a sample of the $CsNO_3Z$ catalyst extracted from a fixed bed reactor after a reaction between soot and active phases of catalysts in an inert helium atmosphere at 360 °C.

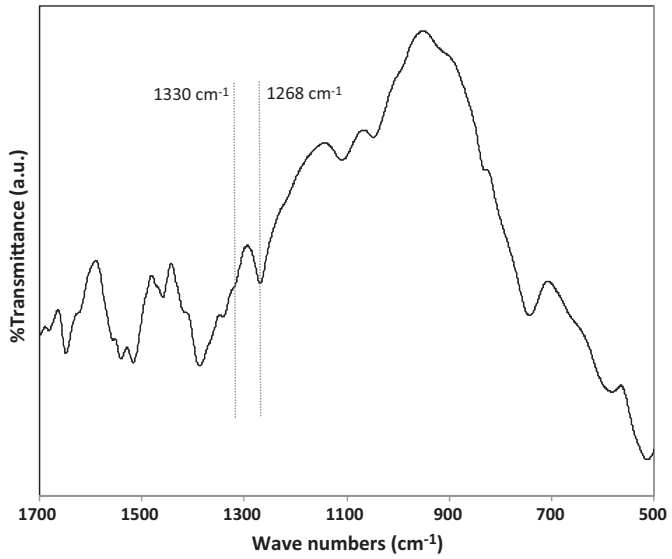


**Fig. 10.** FTIR spectrum of $CsNO_3Z$ catalyst, sample extracted from the reactor after soot combustion at inert atmosphere.

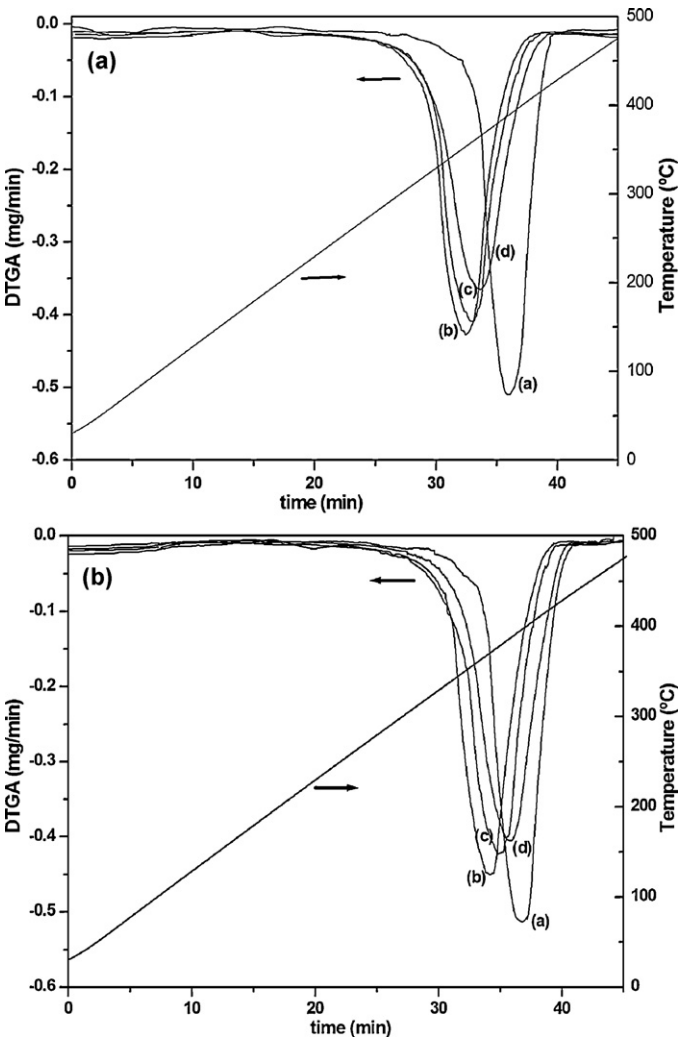


**Fig. 11.** (A) Successive catalytic cycles performed with the $CsNO_3Z$ catalyst: (a) 1st cycle, (b) 2nd cycle, (c) 3th cycle, (d) 4th cycle. (B) Successive catalytic cycles performed with the $CsNO_3$AuZ catalyst: (a) 1st cycle, (b) 2nd cycle, (c) 3th cycle, (d) 4th cycle.

In this FTIR spectrum it is possible to observe an energy absorption band at 1330 $cm^{-1}$ assigned to symmetric N–O stretching and another at 1268 $cm^{-1}$ assigned to antisymmetric N–O stretching of free nitrite species. Besides, other bands appear that can be associated to the presence of coordinated nitrite species. The nitrite cannot be regenerated to nitrate since there is no oxygen in the current that feeds to the reactor. This experiment also evidences that reaction of soot combustion occurs thanks to the oxygen of the nitrate ions. Similar results were reported previously with $KNO_3/ZrO_2$ catalysts [10].

Table 5 and Fig. 8B show results obtained with $CsNO_3$Au/support and $CsNO_3$Au(c)/support catalysts. All catalysts present an initial combustion temperature (between 316 and 334 °C) similar to that observed for $CsNO_3$ catalysts (325 °C). When comparing the temperature of maximum combustion rate of catalysts, it is possible to notice that the gold addition increases the combustion rate when the support is zirconia.

On the other hand, $CsNO_3$Au(c)/support catalysts are more active than $CsNO_3$Au/support catalysts. Probably the little activity increase observed is due to an increase of the cesium nitrate concentration.

On the other hand, to demonstrate that the same samples can repetitively promote the soot oxidation, $CsNO_3Z$ and Au$CsNO_3Z$

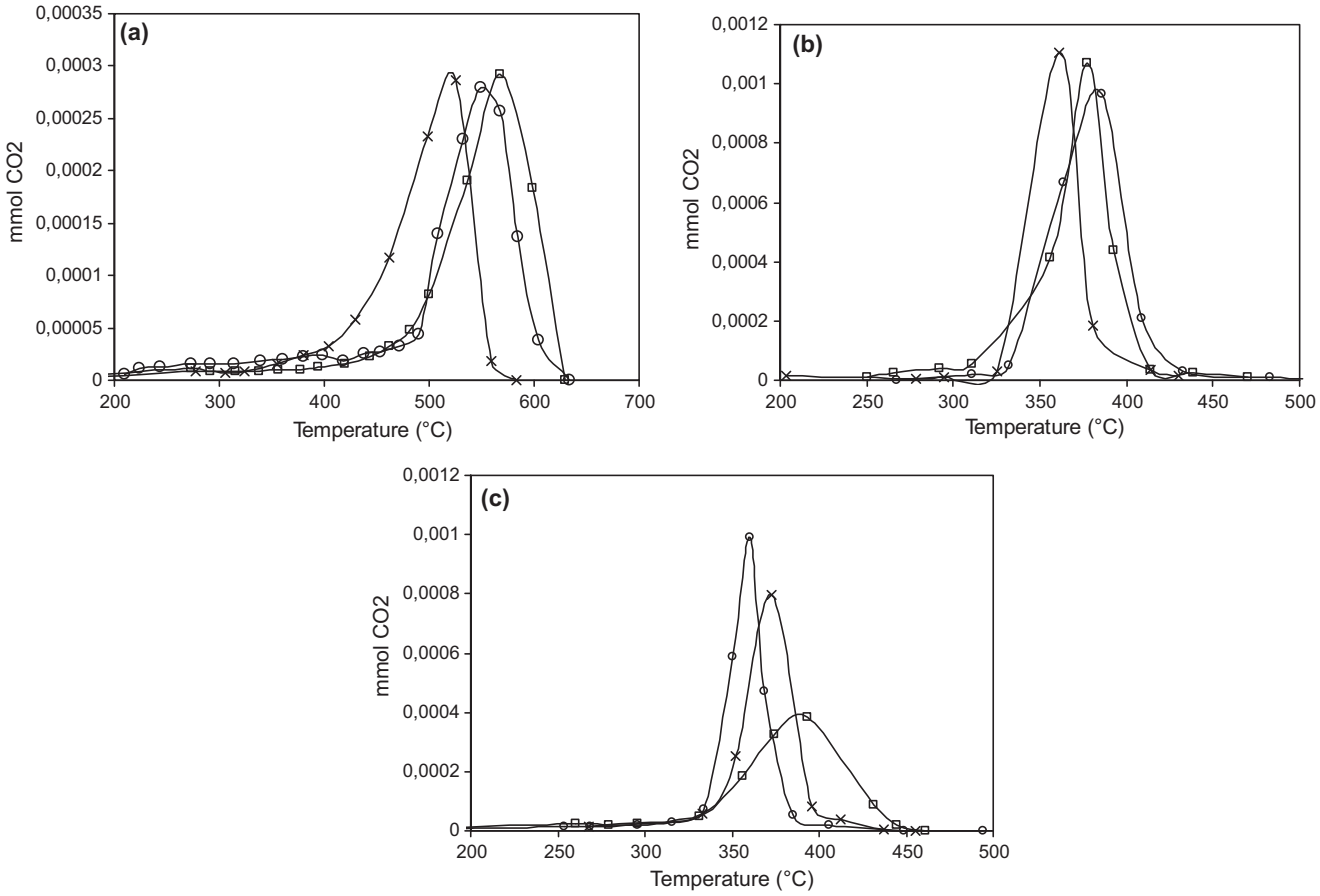


**Fig. 12.** (A) Soot oxidation results of supported Au catalyst-soot (10/1) mixture, "loose contact" in $NO/O_2$/He presence: (x) AuZt, (◯) AuZ, (□) AuS. (B) Soot oxidation results of supported $CsNO_3$ catalyst-soot (10/1) mixture, "loose contact" in $NO/O_2$/He presence: (×) $CsNO_3$Zt, (◯) $CsNO_3$Z, (□) $CsNO_3$S. (C) Soot oxidation results of supported $AuCsNO_3$ catalyst-soot (10/1) mixture, "loose contact" in $NO/O_2$/He presence: (×) $CsNO_3$AuZt, (◯) $CsNO_3$AuZ, (□) $CsNO_3$AuS.

catalysts were used in four successive catalytic cycles (Fig. 11A and B). Both materials show activity after being used several times in reaction evidencing the regeneration and stability of nitrate species and the stability of gold.

### 3.2.2. *Catalytic results obtained in a fixed bed reactor fed with $NO/O_2$*

Experiments were also performed under experimental conditions observed in the exhaust pipe of a diesel engine. For this reason the activity with a gaseous current containing nitrogen oxides is studied and the soot catalyst mixture is made with spatula ("loose contact").

Fig. 12A–C shows catalytic results obtained in a fixed bed reactor fed with a $NO/O_2$ mixture. Curves represent the combustion evolution of particulate matter as function of the temperature. Table 6 shows the NO influence on the temperature corresponding to the maximum combustion rate.

**Table 6**
NO influence in catalytic results obtained in a fixed bed reactor fed with $NO/O_2$/He or O/He with loose contact.

| | $T_{max}$ $NO/O_2$/He | $T_{max}$ $O_2$/He |
|---|---|---|
| Printex-U | 580 | 590 |
| AuS | 567 | 590 |
| AuZ | 549 | 587 |
| AuZt | 526 | 590 |
| $CsNO_3$S | 377 | 475 |
| $CsNO_3$Z | 380 | 370 |
| $CsNO_3$Zt | 360 | 361 |
| $CsNO_3$AuS | 393 | 467 |
| $CsNO_3$AuZ | 360 | 360 |
| $CsNO_3$AuZt | 373 | 380 |

The curve corresponding to the combustion reaction of particulate matter in absence of catalyst shows that the temperature of the maximum is 580 °C in $NO/O_2$ presence and 590 °C in $O_2$ presence.

In both reaction mixtures, $NO/O_2$/He and $O_2$/He, the series of Au catalysts present low activity. The combustion temperature is near the one of the system without catalyst (585 or 590 °C). In NO absence, the catalysts show very low activity. In $NO/O_2$ presence, the catalyst presents some activity and the most active catalyst is the one that presents higher superficial gold concentration, AuZt. The activity can be associated to the gold capacity to adsorb the NO and generate superficial $NO_2$, which is more oxidizing than oxygen and/or nitrate ions. Fig. 13 shows spectra of catalysts Au/supports extracted from the reactor after being used with a $NO/O_2$/He flow. The signal corresponding to the presence of free nitrates at 1385 $cm^{-1}$ is observed in all of them. This signal is more intense in the spectrum of the $Au/ZrO_{2(tetra)}$ catalyst, which is the most active catalyst. These results indicate that the NO presence in the reaction flow originates an activity increase by generation of superficial adsorbed oxo compounds of nitrogen. In this catalyst, NO is coadsorbed with excess oxygen, then the principal species to be expected are $NO_2$ and nitrates ($NO_3^-$) [32].

All catalysts containing in their composition only cesium nitrate present a good activity, with $T_{max}$ between 360 and 380 °C in a $NO/O_2$/He atmosphere or in an $O_2$/He atmosphere, evidencing that the NO addition does not affect substantially the activity of catalysts that contain high cesium nitrate load. Instead, the NO addition generates a reaction rate increase of the $CsNO_3$S catalyst, that con-

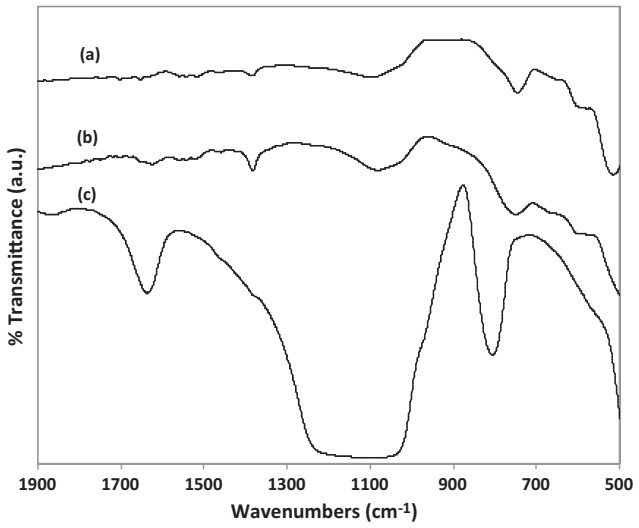


**Fig. 13.** FTIR spectra of catalysts used in the soot combustion reaction with $NO/O_2$/He: (a) AuZ, (b) AuZt, (c) AuS.

tains a low cesium nitrate loading and high cesium concentration. It is suggested that in $NO/O_2$ presence, superficial nitrate species can be generated in situ that can accelerate the reaction.

The gold addition to catalysts that contain cesium nitrate ($CsNO_3$AuSupport) produces a substantial decrease of the cesium nitrate content and still these catalysts exhibit an important activity when the support is zirconia. This decrease in cesium nitrate concentration, when the nitrate concentration is high, does not lead necessarily to an important activity decrease as it was observed in potassium nitrate catalysts supported on zirconia [33]. When the support is silica the nitrate concentration substantially decreases and the activity also decreases.

An interaction between gold and cesium nitrate was observed in TPR experiments where catalysts $CsNO_3$AuZ and $CsNO_3$AuZt present lower reduction temperature than that of catalysts $CsNO_3$Z and $CsNO_3$Zt and this effect is attributed to spill-over of hydrogen. Moreover, the $CsNO_3$AuZ catalyst, the most active of the series $CsNO_3$Au catalysts, with the highest nitrate concentration of its series, presents a noticeable shift in the binding energy of the Au $4f_{7/2}$ signal. Over this support the gold presence increase the activity in $NO/O_2$/He and $O_2$/He presence.

The gold role it is associated to the catalytic selectivity. Catalysts containing only cesium nitrate are active but they give as secondary product CO (2% of $CO_x$). The addition of gold substantially increases the $CO_2$ generation leading a 100% of selectivity to $CO_2$.

## 4. Conclusions

In catalysts $CsNO_3$Z and $CsNO_3$Zt, the cesium nitrate concentration gives results similar to the nominal value.

Instead, the $CsNO_3$S catalyst presents a lower salt concentration suggesting that the anchoring of nitrate species in the silica is weak. All catalysts containing only cesium nitrate present diffraction signals of cesium nitrate. In catalysts that contain cesium nitrate and gold, the cesium nitrate concentration is markedly lower than the nominal value while the cesium concentration is similar to the nominal value. Cesium nitrate has been transformed in cesium chloride as it was observed by XRD.

Analyses by FTIR demonstrate that catalysts with cesium nitrate show energy absorption bands associated to the presence of free nitrate ions.

The surface cesium concentration determined by XPS is higher for catalysts supported on zirconia and the gold addition does not modify the surface cesium concentration. Besides, the surface gold concentration is lower in $CsNO_3$Au/zirconia than in Au/zirconia catalysts.

A synergic effect is noticed between gold and cesium nitrate in TPR experiments. A modification of gold environment by cesium nitrate presence was also observed by XPS. The B.E. value of the Au $4f_{7/2}$ signal for $CsNO_3$AuZ catalyst is shifted in 1.5 eV.

All catalysts containing cesium nitrate exhibit a good activity for soot oxidation using only air in the feed. The reaction mechanism involves a soot oxidation stage by nitrate ion reduction and a second nitrate regeneration stage with oxygen participation of gaseous phase.

New evidences of the nitrite generation were found by thermogravimetric and FTIR analysis.

The most active catalyst for soot combustion in air/He, without NO, and under tight contact condition of the series $CsNO_3$Support is the $CsNO_3$Z catalyst. This catalyst presents large cesium nitrate crystals allowing soot wetting and high nitrate concentration. The gold addition on this catalyst increases the combustion rate and increases substantially the $CO_2$ generation leading the selectivity to 100% in $CO_2$.

All catalysts containing cesium nitrate exhibit good activity in conditions that are near to the real ones: loose contact and NO presence in the feed. The most active catalyst in $NO/O_2$/He presence is $CsNO_3$Zt, which has the lowest temperature of maximum combustion rate, and the addition of gold over this catalyst decreases the combustion rate and the $T_{max}$ increases from 360 to 373 °C. Instead, the addition of gold over the $CsNO_3$Z increases the activity in $NO/O_2$/He presence obtaining a very low $T_{max}$ (360 °C).

The addition of gold results beneficial. All the $CsNO_3$Au catalysts show total selectivity to $CO_2$.

## Acknowledgements

Authors thank for the financial support of UNSL (Universidad Nacional de San Luis), UNLP (Universidad Nacional de La Plata), ANPCYT, CONICET and Ministerio de Ciencia e Innovación, project MAT2009-10481 and FEDER funds. L.R. thanks to the AEIC for funding her staying at Málaga.

## References

[1] R. Jiménez, X. García, C. Cellier, P. Ruiz, A. Gordon, Appl. Catal. A 314 (2006) 81–88.
[2] D. Uner, M.K. Demirkol, B. Dernaika, Appl. Catal. B 61 (2005) 334–345.
[3] D. Fino, G. Saracco, V. Specchia, Chem. Eng. Sci. 57 (2002) 4955–4966.
[4] Q. Li, M. Meng, Z. Zou, X. Li, Y. Zha, J. Hazard. Mater. 161 (2009) 366–372.
[5] I. Atribak, A. Bueno-López, A. García-García, P. Navarro, D. Frías, M. Montes, Appl. Catal. B 93 (2010) 267–273.
[6] J. Liu, Z. Zhao, C. Xu, A. Duan, L. Zhu, X. Wang, Catal. Today 118 (2006) 315–322.
[7] B.A.A.L. van Setten, J.M. Schouten, M. Makkee, J.A. Moulijn, Appl. Catal. B 28 (2000) 253–257.
[8] P. Ciambelli, M.D. Amore, V. Palma, S. Vaccaro, Combust. Flame 99 (1994) 413–421.
[9] R. López-Fonseca, U. Elizundia, I. Landa, M.A. Gutiérrez-Ortiz, J.R. González-Velasco, Appl. Catal. B 61 (2005) 150–158.
[10] I.D. Lick, A. Carrascull, M.I. Ponzi, E.N. Ponzi, Ind. Eng. Chem. Res. 47 (2008) 3834–3839.
[11] A.L. Carrascull, I.D. Lick, E.N. Ponzi, M.I. Ponzi, Catal. Commun. 4 (2003) 124–128.
[12] D. Hleis, M. Labaki, H. Laversin, D. Courcot, A. Aboukaïs, Colloid Surf. A: Physicochem. Eng. Aspects 330 (2008) 193–200.
[13] Y. Zhang, X. Zou, Catal. Commun. 7 (2006) 523–527.
[14] A. Carrascull, C. Grzona, I. Lick, M. Ponzi, E. Ponzi, React. Kinet. Catal. Lett. 75 (2002) 63–68.
[15] B. Bialobok, J. Trawczynski, T. Rzadki, W. Mista, M. Zawadzki, Catal. Today 119 (2007) 278–285.
[16] X. Wu, D. Liu, K. Li, D. Weng, Catal. Commun. 8 (2007) 1274–1278.
[17] N. Galdeano, A. Carrascull, M. Ponzi, I. Lick, E. Ponzi, Thermochim. Acta 421 (2004) 117–121.
[18] Y. Zhang, Y. Qin, X. Zou, Catal. Commun. 8 (2007) 1675–1680.
[19] H. An, P.J. McGinn, Appl. Catal. B 62 (2005) 46–56.
[20] M. Haruta, T. Kobayashi, H. Sano, N. Yamada, Chem. Lett. 16 (1987) 405–408.

[21] Masatake Haruta, Chem. Rec. 3 (2003) 75–87.
[22] R.J.H. Grisel, B.E. Nieuwenhuys, Catal. Today 64 (2001) 69–81.
[23] M.C. Soares, M. Bowker, Appl. Catal. A 291 (2005) 136–144.
[24] C.W. Corti, R.J. Holliday, D.T. Thompson, Appl. Catal. A 291 (2005) 253–261.
[25] G. Pattrick, E. van der Lingen, C.W. Corti, R.J. Holliday, D.T. Thompson, Top. Catal. 30–31 (2004) 273.
[26] A.F. Wells, Structural Inorganic Chemistry, Oxford Univ. Press, N.Y., 1986, p. 542.
[27] C.N.R. Rao, J. Gopalakrishnam, New Directions in Solid State Chemistry, Cambridge Univ. Press, London, 1986.
[28] K. Nakamoto, Infrared and Raman Spectra of Inorganic and Coordination Compounds, Wiley Interscience Publication, John Wiley and Sons, Inc., N.Y., 1997.
[29] M. Hirata, H. Monjyuchiro, R. Sekine, J. Onoe, H. Nakamatsu, T. Mukoyama, H. Adachi, K. Takeuchi, J. Electron Spectrosc. 83 (1997) 59–64.
[30] J.F. Moulder, W.F. Stickle, P.E. Sobol, K.D. Bomben, Standard Spectra for Identification and Interpretation of XPS Data, Perkin Elmer, Eden Prairie, MN, 1992.
[31] S. Mosconi, I. Lick, A. Carrascull, M. Ponzi, E. Ponzi, Catal. Commun. 8 (2007) 1755–1758.
[32] K.I. Hadjiivanov, Catal. Rev. Sci. Eng. 42 (2000) 71–144.
[33] A. Carrascull, M.I. Ponzi, E.N. Ponzi, Ind. Eng. Chem. Res. 42 (2003) 692–696.